

1 **Sources and Long-term Variability of Carbon Monoxide at**
2 **Mount Kenya and in Nairobi**

3 Leonard Kirago¹, Örjan Gustafsson¹, Samuel M. Gaita¹, Sophie L. Haslett¹, Michael J. Gatari²,
4 Maria E. Popa³, Thomas Röckmann³, Christoph Zellweger⁴, Martin Steinbacher⁴, Jörg
5 Klausen⁵, Christian Félix⁵, David Njiru⁶, and August Andersson^{1*}

6 ¹Department of Environmental Science, and the Bolin Centre for Climate Research, Stockholm University, 10691
7 Stockholm, Sweden

8 ²Institute of Nuclear Science & Technology, University of Nairobi, 31907-00100 Nairobi, Kenya

9 ³Institute for Marine and Atmospheric research Utrecht (IMAU), Utrecht University, Utrecht 3584CC, The
10 Netherlands

11 ⁴Empa, Swiss Federal Laboratories for Materials Science and Technology, Laboratory for Air
12 Pollution/Environmental Technology, 8600 Dübendorf, Switzerland

13 ⁵Federal Office of Meteorology and Climatology MeteoSwiss, CH-8058 Zurich, Switzerland

14 ⁶Kenya Meteorological Department, Nairobi, Kenya

15 *Correspondence to: August Andersson (august.r.andersson@gmail.com)

16 **Abstract.** Carbon monoxide (CO) concentrations in the troposphere are decreasing globally, with Africa as an
17 exception. Yet, the region is understudied, with a deficit of ground-based observations and highly uncertain CO
18 emission inventories. This paper reports multi-year observational CO data from the Mt. Kenya Global Atmosphere
19 Watch (GAW) station, as well as summertime CO isotope observations from both Mt. Kenya and Nairobi, Kenya.
20 The CO variability at Mt. Kenya is characterized by slightly increased concentrations during dry periods and a
21 strong influence of short-term pollution events. While some data gaps and differences in instrumentation
22 complicate decadal-scale trend analysis, a small long-term increase is resolved. High pollution events are
23 consistent with isotopic signal from downwind savanna fires. The isotope fingerprint of CO in Nairobi indicate an
24 overwhelming dominance (near 100%) of primary emissions from fossil fuel combustion with implications for air
25 pollution policy. In contrast, the isotope signature of CO intercepted at the large footprint Mt. Kenya region
26 suggests at least 70% primary sourced, with a predominance likely from, savanna fires in Africa. Taken together,
27 this study provides quantitative constraints of primary vs secondary CO in the eastern Africa region and in urban
28 Nairobi, with implications for satellite-based emission inventories as well as for chemical-transport and climate-
29 modelling.

30 1. Introduction

31 Carbon monoxide (CO) is the dominant sink for the hydroxyl radical (OH), accounting for over 50% consumption
32 of OH in the atmosphere (Lelieveld et al., 2016). It therefore influences the atmosphere's oxidation and cleansing
33 capacity and, by extension, chemically regulates the atmospheric lifetime and abundance of other reactive gases
34 such as methane and halocarbons (Lelieveld et al., 2016; Zheng et al., 2019). As such, CO is an indirect greenhouse
35 gas with a net positive warming effect on climate (Szopa et al., 2021). In addition to climate effects, CO is a
36 precursor to the formation of ground-level ozone, with implications for human health (Chen et al., 2021; WHO,
37 2016; Zhang et al., 2019). Anthropogenic activities such as biomass burning and fossil fuel combustion are
38 important contributors to the global CO budget, in addition to atmospheric reactions, e.g., oxidation of
39 hydrocarbons (Duncan et al., 2007; Zheng et al., 2019). However, the CO source contributions, mole fractions,
40 and atmospheric residence time are spatially variable, complicating the source-sink assessment.

41 Global CO levels have been declining over the past two decades, but Africa is an exception. The key source of
42 information on CO trends in the African region is satellite-based observations that show an increase in CO mole
43 fractions (Buchholz et al., 2021; Hedelius et al., 2021; Zheng et al., 2019). However, the ground-truthing of the
44 satellite observations is challenged by a deficit of atmospheric observatories and scant continuous long-term
45 observations in the region (DeWitt et al., 2019; Henne et al., 2008b; Kulmala, 2018). Exacerbating this
46 observational deficit, regional CO emission inventories are not well-defined as the continent possesses a unique
47 CO emission profile, different from other regions such as Europe and South Asia (Crippa et al., 2018; Dasari et
48 al., 2021; Hedelius et al., 2021). To advance our understanding of trends in CO over Africa and its source
49 contributions, long-term CO measurements and isotope-based source apportionment studies are required but data
50 availability is scarce.

51 The isotopic composition of CO provides insights into the relative strengths of regional CO sources and
52 atmospheric processing (Brenninkmeijer, 1993; Dasari et al., 2021; Henne et al., 2008b; Röckmann et al., 2002).
53 A particular source of CO possesses a characteristic isotopic signature, with the isotopic composition of the
54 ambient CO reflecting that of the combined sources, sinks, and atmospheric ageing (Brenninkmeijer and
55 Röckmann, 1997; Dasari et al., 2021; Popa et al., 2014; Röckmann et al., 1998, 2002). For example, CO from
56 primary sources (fossil combustion and biomass burning) has a more enriched $\delta^{18}\text{O}$ signature (above +12‰)
57 compared to that of secondary-formed CO, e.g., from oxidation of CH_4 (at ~0‰) and non-methane hydrocarbons
58 (NMHC), at $\sim 2.4 \pm 2.4\text{‰}$ (Brenninkmeijer and Röckmann, 1997).

59 Additional source information can be obtained from the $\delta^{13}\text{C}$ signatures. CO formed from methane oxidation is
60 strongly depleted in ^{13}C ($\delta^{13}\text{C} = -51.9 \pm 1.6\text{‰}$) in contrast to, for example, CO emitted from burning of C_4 plants
61 ($\delta^{13}\text{C} = -14.0 \pm 3.8\text{‰}$), C_3 plants ($\delta^{13}\text{C} = -26.9 \pm 4.9\text{‰}$) or fossil combustion at $-27.8 \pm 1.5\text{‰}$ (Brenninkmeijer et
62 al., 1999). However, the kinetic isotope effect (KIE) during the CO-OH reaction (the main atmospheric CO
63 removal mechanism) results in the enrichment of $\delta^{13}\text{C}$ by 4-5‰ and more depleted $\delta^{18}\text{O}$ signatures (by ~10‰) in
64 the lower troposphere (Brenninkmeijer et al., 1999; Röckmann et al., 1998). Overall, isotope forensics can provide
65 valuable data on CO emissions in remote and urban locations in Africa, especially considering that the region is
66 largely understudied, with very few ground-based CO observations and highly uncertain emission inventories.

67 This study investigates the long-term trends in CO mole fractions at Mt. Kenya GAW station, a high-altitude
68 monitoring site in equatorial East Africa well suited to intercept the regional emission footprint. Online CO mole
69 fractions measurements have been going on at the observatory since 2002, albeit with large data gaps due to
70 technical challenges. Flask-based measurements carried out at Mt. Kenya at different periods by NOAA (2003-
71 2011) were used for gap filling. The online and NOAA flask-measured CO data were obtained from the WMO's
72 World Data Centre for Greenhouse Gases (WDCGG) database. After the CO measurements from Cape Point,
73 South Africa, this is likely the longest-running data available in sub-Saharan Africa and provides observational
74 constraints of the region's long-term trend in CO. The present study additionally provides stable isotope
75 composition data of CO to resolve source attribution of the observed higher summertime CO amount fraction.
76 Furthermore, the data are compared to previously obtained and unpublished isotope data from Mt. Kenya (1996-
77 1997; earlier unpublished work by Röckmann and Brenninkmeijer) and that of an urban site in Nairobi in summer
78 2021 to provide further insights into regional CO sources. This dataset is unprecedented in the region and facilitates
79 improved understanding of the regional CO emission trends and source attribution.

80 **2. Methodology**

81 **2.1 Measurement sites**

82 Ambient air sampling was conducted at a remote mountain site, the Mt. Kenya Global Atmospheric Watch (GAW)
83 station, and in Nairobi city. The Mt. Kenya GAW station is located on the north-western slope of Mt. Kenya (0.062
84 °S, 37.297 °E, at 3678 m MSL) in eastern equatorial Africa. The station description, site selection and
85 representativeness, and meteorological characterization are detailed by Henne et al. (2008a, 2008b). In brief, the
86 station lies within a nature conservancy, the Mount Kenya National Park, and contributes to the World
87 Meteorological Organization GAW programme. The closest human settlements and roadways are over 17 km
88 away, and the nearest town (Nanyuki) is at 1900 m MSL. A small touristic infrastructure, the Old Moses Camp, is
89 situated 300 m below and ca. 1.9 km to the NNW of the station. The second site, in the megacity of Nairobi,
90 Kenya, was a rooftop measurement site (~17 m above ground level; 1690 m asl.; 1.279° S, 36.817° E). As described
91 previously, the Nairobi site is representative of the city's ambient conditions (Kirago et al., 2022b).

92 **2.2 Ambient air sampling**

93 Glass flask sampling was conducted in August 2021 at the Mt. Kenya GAW station and in Nairobi with an in-
94 house assembled portable sampler consisting of a diaphragm pump (KNF Neuberger N86E) connected with 1/4"
95 Dekabon tubing. The sampler design, glass flask pre-conditioning protocol and sampling procedure are previously
96 described (Dasari et al., 2021). Briefly, the sampler was designed to fill two pre-conditioned glass flasks (Normag,
97 1L) simultaneously, that is, each sample was collected in duplicates. Ambient air was drawn at a flow rate of 2 L
98 min⁻¹ and dried through a magnesium perchlorate trap. First, the glass flasks were flushed for 20 minutes before
99 compressing the dried air to an absolute pressure of ~1.7 bar. At Mt. Kenya GAW station, 21 nighttime (02:00h
100 local time) and six daytime (14:00h local time) air sample sets were collected. Nine sample pairs were collected
101 in Nairobi (every second day; daytime only; 14:00h local time). The filled glass flasks were sent to the Institute
102 for Marine and Atmospheric Research Utrecht (IMAU), Utrecht University, for processing and stable isotope
103 analysis of CO.

104 2.3 Measurements of CO mole fractions and stable isotopes ($\delta^{18}\text{O}$ and $\delta^{13}\text{C}$) composition of CO

105 The CO mole fraction and stable isotopic composition measurements of the collected glass flask samples were
106 performed at IMAU, Utrecht University. A continuous-flow isotope ratio mass spectrometry (CF-IRMS, Thermo
107 Scientific Delta V Advantage) system was used, applying a previously described measurement protocol (Pathirana
108 et al., 2015). In brief, the sample gas was introduced into the analytical system using an automated multi-port unit,
109 via a mass flow controller and under ultra-high-purity helium flow. Here, the air sample was directed through a
110 trap with Ascarite (8 - 20 mesh, Thermo Scientific™) followed by magnesium perchlorate (Sigma-Aldrich), to
111 remove CO_2 and water. A subsequent cryogenic trap (liquid N_2 , -196°C) was used to remove the remaining traces
112 of CO_2 , N_2O and hydrocarbons. The CO in the clean air matrix was then oxidized to CO_2 using Schütze reagent
113 ($\text{I}_2\text{O}_5/\text{H}_2\text{SO}_4$ mixture on granular silica gel) synthesized in-house. Subsequently, the CO-derived CO_2 was cryo-
114 trapped in liquid- N_2 , while other residual gases (e.g., O_2 and N_2) were pumped out. The sample was further purified
115 on a GC column, dried via a Nafion dryer, and subsequently transferred to the CF-IRMS via an open split inlet for
116 stable isotopes ($\delta^{18}\text{O}$ and $\delta^{13}\text{C}$) analysis.(Pathirana et al., 2015) The original CO amount fraction was deduced
117 from the quantity of the derived CO_2 .

118 The isotopic composition is expressed as per mil (‰) enrichment or depletion of the isotope ra-tio in the sample
119 relative to that of international standard materials, which in these cases are the Vienna PeeDeeBelemnite (V-PDB)
120 standard for $\delta^{13}\text{C}$ -CO, and the Vienna Standard Mean Ocean Water (V-SMOW) for $\delta^{18}\text{O}$ -CO measurements
121 (Brenninkmeijer et al., 1999; Pathirana et al., 2015). A reference cylinder with atmospheric air with known isotopic
122 composition and mole fraction ($\delta^{13}\text{C} = -30.25\text{‰}$; $\delta^{18}\text{O} = +7.10\text{‰}$; $\text{CO} = 180$ ppb) was used for calibration.
123 Periodical measurements of "target" gases were used to monitor the precision and accuracy of the measurements,
124 as well as the long-term stability of the analytical system (Pathirana et al., 2015). In addition, blank runs (without
125 injecting the sample or reference gas) were performed to assess the background CO_2 , mainly from the Schütze
126 reagent. The typical 1-sigma measurement reproducibility during the time of these analyses is estimated at 0.12‰
127 for $\delta^{13}\text{C}$ and 0.16‰ for $\delta^{18}\text{O}$.

128 2.4 Sampling and isotopic characterization of CO for the 1996/97 campaign

129 High-volume air samples were collected between July and September 1996 on an exploratory mission around
130 Mount Kenya following the ring road A2/B6, and branching off towards the mountain to locations where sufficient
131 power was available for sample collection. During this campaign and later incidental samplings in 1997 air samples
132 of approximately 500 L volume were compressed into 5 L aluminium cylinders using a modified RIX compressor
133 (Mak and Brenninkmeijer, 1994). Unfortunately, records of precise locations have been lost. The filled cylinders
134 were sent to the Max Planck Institute for Chemistry in Mainz, Germany, for CO isotope analysis on a high-volume
135 extraction unit (Brenninkmeijer et al., 1999; Röckmann et al., 2002). A high CO concentration calibration gas (269
136 ppm) that was used during the 1996/7 measurements has been preserved and is regularly measured in the lab of
137 Utrecht University to assure scale compatibility.

138

139 2.5 Long-term CO mole fractions at the Mt. Kenya GAW station

140 High-resolution CO data from Mt. Kenya GAW station are available from the WMO World Data Centre for
141 Greenhouse Gases (WDCGG; <https://gaw.kishou.go.jp/>). A continuous time series is available for the 2002-2006
142 and 2020-2021 periods, with some large gaps attributable mainly to power outages and data quality issues.
143 Between 2010 and 2015, the station was disconnected from the power grid following a bush fire, while
144 performance audits revealed the CO analyzer to be in poor working condition between 2015-2019
145 (decommissioned in 2020), compromising the data quality (Zellweger et al., 2020). Over time, the CO
146 measurements were made using different CO analyzers (Thermo Electron Corporation TEI 48C-TL in 2002-2006,
147 Horiba APMA360 in 2010-2019, and Picarro G2401 in 2020-2021).

148 The instrument calibration, quality control protocols, and data treatment procedures are discussed elsewhere
149 (Henne et al., 2008b; Zellweger et al., 2009, 2020). In brief, ambient air was drawn into the CO instrument using
150 1/4" Teflon (till 2019) and 1/4" Synflex 1300 (after 2019) tubings at a flow rate of 4 l/min via a Nafion drier to
151 remove moisture and a particulate filter. The air inlet was about 7 m above ground and protected against rain, snow
152 and direct wind. These instruments were installed and calibrated by the Swiss Federal Institute for Materials
153 Science and Technology (Empa) in collaboration with the Federal Office of Meteorology and Climatology
154 MeteoSwiss, and operated by the Kenya Meteorological Department (KMD). The instrument calibration and
155 performance audits are conducted regularly by the GAW World Calibration Center hosted at Empa (Zellweger et
156 al., 2020). In addition, flask-based CO data from Mt. Kenya GAW station by NOAA Global Monitoring labora-
157 tory and published in the WDCGG database was used in this study (Petron, 2023).

158 2.6 Trajectory and statistical modelling

159 The air mass back trajectories (10 days; arrival height of 100 m above ground level) were calculated to identify
160 the air mass source region. The NOAA Hybrid Single-Particle Lagrangian Integrated Trajectory model (HYSPPLIT,
161 version 4) and GDAS ($1^\circ \times 1^\circ$) archived meteorological datasets were used (Stein et al., 2015). The Bayesian
162 Markov chain Monte Carlo (MCMC) model was used to quantitatively constrain CO fractional contributions and
163 account for source end member variability and measurement uncertainties (Dasari et al., 2021). The MCMC
164 simulations were carried out with MATLAB R2020 with 1,000,000 runs and 10,000 runs for sample burn-in and
165 a data thinning of 100.

166 3. Results and Discussion

167 3.1 CO mole fractions at Mt. Kenya GAW Station and Nairobi

168 The results of the CO observations at Mt. Kenya GAW station, both online and flask measurements, are presented
169 in Figure 1. Part of the data (2002 - 2006) has been comprehensively discussed previously (Henne et al., 2008b).
170 Overall, peak CO mole fractions were observed during the dry periods (SI Figure S1). Assessment of the long-
171 term CO trend, following the approach by Thoning and Tans (1989), reveal a small but statistically significant
172 positive decadal trend of 6.7 ± 0.4 ppb/10yrs. This statistical model is based on a fit function that includes a linear
173 term, a quadratic term, as well as first and second harmonics. For comparison, simple linear regression gives a

174 similar decadal rate of 6.2 ± 0.6 ppb/10yrs (for uncertainty estimation, see Kirago et al., 2022a). Like many types
175 of environmental data, the present CO data display a lognormal-like concentration distribution, suggesting
176 influence by exponential processes such as sink kinetics (Andersson, 2021). This may influence trend analysis.
177 Similarly to linear regression, regression of log-transformed data also gives a significant positive rate, which
178 suggests that the skewed concentration profile has little influence on trend estimation. However, given the large
179 data gaps and different measurement techniques, such interpretations should not be over-emphasized.
180 Nevertheless, the increasing trend here constrained for ground observations of CO is qualitatively consistent with
181 satellite retrievals and model estimates for sub-Saharan Africa (Buchholz et al., 2021; Hedelius et al., 2021; Zheng
182 et al., 2019).

183 The observed CO levels, ranging between 55 – 250 ppb, are comparable to those previously recorded at Mt. Kenya
184 station (Henne et al., 2008b), but lower than CO concentrations reported at the Rwanda Climate Observatory -
185 another remote site also in Eastern Africa, possibly with a stronger and more direct influence of savanna burning
186 episodes (DeWitt et al., 2019). The daytime and nighttime ambient flask CO concentrations were comparable,
187 similar to observation from Picarro-measured CO measurements though with a slight daytime elevation (SI Figure
188 S1). During the nighttime, the station stands above the atmospheric boundary layer, hence reduced influence from
189 local sources. Overall, changes in source strength, air mass transport pathways and meteorological parameters such
190 as planetary boundary layer thickness are likely to be key drivers of the observed temporal variations. In Nairobi,
191 the CO concentrations during August 2021 range between 200 – 700 ppb ($\sim 0.2 - 0.8$ mg m⁻³, assuming average
192 weather conditions), well within the WHO recommended short-term (24-h average) air quality guideline level of
193 4 mg m⁻³ (WHO, 2021). While CO is not a major direct health concern in Nairobi nor in other urban settings
194 (Chen et al., 2021), it affects the presence of health-detrimental components such as ground-level ozone and
195 secondary aerosols.

196 Back-trajectories calculated with the HYSPLIT model were combined with the CO data to learn more about source
197 regions incident with elevated CO mole fractions. Air masses originating from different geographical areas, such
198 as from eastern Africa, Arabian Peninsula, northern Africa, South Asia, and south-eastern Africa, as well as cleaner
199 air masses from the Indian Ocean, are intercepted at Mt. Kenya GAW station (Figure 2). This underlines the
200 suitability of Mt. Kenya GAW station to capture both the regional and intercontinental footprints. The elevated
201 summertime (June - August) CO mole fractions are linked to the arrival of south-easterly air masses, coinciding
202 with large-scale savanna fires in southern Africa and Madagascar. The air masses shift north-easterly during winter
203 (December - March), and coincide with savanna fires in northern Africa (Andersson et al., 2020; Kirago et al.,
204 2022a). Although the intercepted air masses do not directly flow over West-Central Sub-Saharan Africa, where
205 most fires occur, the atmospheric residence time of CO is sufficient for regional and intercontinental mixing. Air
206 masses with elevated CO loadings from South Asia and the Arabian Peninsula are also intercepted during winter.
207 High wintertime CO amount fractions have been reported from a South Asian receptor site in the northern Indian
208 Ocean (Dasari et al., 2021). Taken together, the seasonal variability in CO mole fraction can partly be explained
209 by regional emission events, combined with a contribution from other geographical source regions such as South
210 Asia.

211 3.2 Isotopic constraints of sources to CO from Mount Kenya and Nairobi

212 The stable isotope composition of CO ($\delta^{13}\text{C}$ and $\delta^{18}\text{O}$) for ambient samples from Mt. Kenya GAW station during
213 August 2021 varied temporally with the CO mole fractions (SI Figure S2). The $\delta^{13}\text{C}$ ranged between -31.5‰ to -
214 28.0‰, while $\delta^{18}\text{O}$ ranged between 2.5 to 10.0‰ (SI Figure S2). However, there were no distinct temporal or
215 diurnal trends in the recorded isotopic values (both daytime and night-time samples were measured). The air
216 masses were consistently southeasterly during the three weeks study period (SI Figure S3). Comparable $\delta^{18}\text{O}$
217 composition was observed in 1996/97 samples (ranged between 3.7 to 10.4‰), but was more enriched in $\delta^{13}\text{C}$ (-
218 28.4‰ to -26.6‰). The isotopic composition in the Mt. Kenya background region was distinct from that of the
219 urban Nairobi location that recorded highly enriched $\delta^{18}\text{O}$ values ($17.5 \pm 2.2\%$; SI Figure S2).

220 The Keeling plot approach provides insights into the regional CO sources. Here, a linear relationship is observed
221 between the isotope signatures and the inverse of the CO amount fractions ($\delta^{13}\text{C}$ vs $1/[\text{CO}]$ and $\delta^{18}\text{O}$ vs $1/[\text{CO}]$)
222 both at Mt. Kenya and in Nairobi (Figure 3). This implies that the CO dynamics in this system can be described
223 by a two-component mixture; a relatively stable background fraction and a regional varying source (Dasari et al.,
224 2021; Keeling, 1958). The y-axis intercept in this relation represents the source signature. At Mt. Kenya, analysis
225 of the recently-obtained dataset (2021) reveals the stable isotopes signature of the source of $\delta^{18}\text{O} = 14.0 \pm 1.2\%$
226 and $\delta^{13}\text{C} = -27.7 \pm 0.6\%$. For the samples collected during the 1996/97 campaign, the $\delta^{18}\text{O}$ signature is very similar
227 and indistinguishable ($\delta^{18}\text{O} = 14.2 \pm 2.1\%$), while the source is more enriched in ^{13}C ($\delta^{13}\text{C} = -24.7 \pm 0.7\%$; Figure
228 4). The latter suggests differences in the relative strengths of the contributing sources, possibly a relatively higher
229 contribution from C_4 plants burning or a relatively smaller influence of secondary CO from atmospheric reactions
230 during the 1996/97 campaign. It should be kept in mind that the 1990s samples were obtained at a lower altitude
231 location on the slopes of Mt. Kenya. C_4 plants like maize and sugarcane are commonly grown in Kenya, while also
232 biomass usage (including crop residuals for household energy) and agricultural burning are prevalent in the region
233 (World Bank, 2011). In Nairobi, a clearly distinct source signature is noted, especially for $\delta^{18}\text{O}$ ($\delta^{13}\text{C} = -26.0 \pm$
234 0.4% and $\delta^{18}\text{O} = 22.9 \pm 0.8\%$; Figures 4). The highly enriched $\delta^{18}\text{O}$ source signature in Nairobi indicates almost
235 exclusively high temperature combustion sources, while a mixed source regime (both combustion sources and CO
236 emanating from atmospheric reactions) is observed at Mt. Kenya; these can be quantitatively resolved using an
237 isotopic mass balance approach

238 The source signatures can be used to quantitatively constrain the fractional contributions of CO in the regional
239 background and urban atmosphere (Dasari et al., 2021). However, information was available for only two isotopes,
240 $\delta^{13}\text{C}$ and $\delta^{18}\text{O}$, against five potential sources that can contribute to the overall CO isotopic signature (C_3 plants,
241 fossil, C_4 plants, CH_4 oxidation and NMHC oxidation), yielding a mathematically under-determined scenario.
242 Furthermore, the weak linear correlation for $\delta^{13}\text{C}$ in the Keeling plot ($\delta^{13}\text{C}$ vs $1/[\text{CO}]$; $R^2 = 0.34$ for Mt. Kenya)
243 limits its application in the statistical model. Therefore, only $\delta^{18}\text{O}$ signatures were here modelled ($R^2 = 0.64$ for
244 both Mt. Kenya; $R^2 = 0.89$ for Nairobi; $P < 0.05$). Hence, the CO sources were partitioned into two major classes:
245 primary/combustion (fossil, C_3 and C_4 biomass) and secondary (i.e., oxidation of methane and NMHC).

246 A Bayesian statistical model, drawing upon the model described in Dasari et al. (2022), was used to estimate the
247 contribution of secondary ($f_{\text{secondary}}$) vs primary (f_{primary}) CO sources. In this model the relative contributions of
248 primary vs. secondary CO for the temporally varying source is computed, corresponding to the $\delta^{18}\text{O}$ values at the
249 limit where $1/\text{CO}$ approaches zero (the $\delta^{18}\text{O}$ intercept in the Keeling plot). First, the source end members for the

250 two fractions were established. Unlike the oxidation of NMHC, the CH₄-oxidized CO fluxes have little variability
251 (CH₄ has a long atmospheric lifetime) and largely contribute to the background signal (Dasari et al., 2021; Worden
252 et al., 2019; Zheng et al., 2019). Therefore, the temporally-varying secondary CO end member was assigned that
253 of the NMHC oxidation source ($\delta^{18}\text{O}_{\text{secondary}} = 2.4 \pm 2.4\text{‰}$).

254 The primary CO end member is a composite of the three combustion sources; C₄ biomass ($+20.2 \pm 4.9\text{‰}$), C₃
255 biomass ($+16.3 \pm 5.1\text{‰}$) and fossil fuel combustion at $+19.2 \pm 4.9\text{‰}$ (Dasari et al., 2021). Although the relative
256 contributions are uncertain, the $\delta^{18}\text{O}$ end members largely overlap. Model estimates show biomass burning in
257 Africa accounts for 80 - 90% of the surface CO emissions (Zheng et al., 2018). Similar contributions to black
258 carbon (different but co-emitted incomplete combustion product) were observed using isotopic constraints with
259 near-equal contributions from C₃ and C₄ biomass in the eastern Africa background atmosphere (Kirago et al.,
260 2022c). Therefore, the relative source contributions were estimated at 50% from C₃ biomass and 50% from C₄ and
261 fossil sources at Mt. Kenya. Hence, a primary CO end member was established at $\delta^{18}\text{O}_{\text{primary}} = 18.4 \pm 3.5\text{‰}$. In
262 Nairobi, fossil fuel combustion was estimated to contribute to 85% of the CO emission in the city ($\delta^{18}\text{O}_{\text{primary}} =$
263 $+19.2 \pm 4.9\text{‰}$). Since primary source endmembers largely overlap, the model simulations were generally insen-
264 sitive to chosen priors, as investigated by sensitivity analysis.

265 A similar $\delta^{18}\text{O}$ source signature ($\sim 14.0 \pm 2.1\text{‰}$) was observed at the two Mt. Kenya campaigns (1996/97 and
266 2021). Applying the established endmembers, we estimate the contribution of CO from primary/ combustion
267 sources at the regional background site to be at least 70%. In contrast, we found an almost exclusively primary CO
268 component for the urban Nairobi case. Nairobi is a strong air pollution source region, and the CO loadings largely
269 reflect the city's CO emissions. CO is, e.g., a precursor to low-level ozone, and thus emissions deteriorate air
270 quality. Present findings show that air quality policy should target primary emissions, especially from traffic
271 (Kirago et al., 2022b). In contrast, Mt. Kenya GAW station captures a more regional footprint with a dominant
272 contribution from savanna fires.

273 **4. Conclusion**

274 This study provides ground-observational constraints that broadly supports earlier suggestions that savanna fires
275 are the main emitters and modulators of CO loadings over Sub-Saharan Africa. Although the data gaps in CO
276 mixing ratios and mixed instrumentation complicates detailed analysis, a small decadal increase of 6.7 ± 0.4
277 ppb/10yrs was resolved for the Mt. Kenya GAW station, in agreement with satellite observations and emission
278 inventories for the Sub-Saharan region (Buchholz et al., 2021; Hedelius et al., 2021; Zheng et al., 2019). Isotope-
279 based source apportionment shows that at least two thirds of the CO emitted from East African savanna fires are
280 of primary origins, while for Nairobi primary sources approach 100%. The latter has implications for air quality
281 policy, suggesting primary emissions such as traffic should be targeted, in line with previous findings for BC
282 (Kirago et al., 2022b). These findings put constraints on satellite-based emission inventories and chemical-
283 transport and climate modelling. Overall, this study corroborates earlier findings that in order to reduce the
284 secondary climate warming effect from CO over Sub-Saharan Africa, man-made savanna fires should be reduced
285 (Andersson et al., 2020).

286

287 **Acknowledgement**

288 This work was supported by research grants from the Swedish Research Council (VR contracts nos. 2013-114,
289 2017-05687 and 2020-05384), the Swedish Research Council for Sustainable Development (FORMAS contract
290 no. 2020-01951), and the Swedish Research Council Distinguished Professor Grant (VR contract no. 2017-
291 01601). Sample analysis was supported by the research grants from European Commission under the Horizon
292 2020 – Research and Innovation Framework Programme, H2020-INFRAIA-2020-1 (grant agreement number
293 101008004).

294 We commend the efforts of the Kenya Meteorological Department (KMD), the Swiss Federal Institute for
295 Materials Science and Technology (Empa), and the Federal Office of Meteorology and Climatology MeteoSwiss
296 for Mt. Kenya GAW Station operations. We appreciate the field and technical support from the staff at the Institute
297 of Nuclear Science & Technology, University of Nairobi and KMD. We commend Prof. Carl Brenninkmeijer and
298 Sergey Gromov for their contribution to science, and contribution to 1996/97 campaign/ data used in this
299 manuscript.

300 We acknowledge the use of data from the World Data Centre for Greenhouse Gases (WDCGG) database
301 (<https://gaw.kishou.go.jp/>), hosted by the World Meteorological Organization. The authors gratefully acknowledge
302 the NOAA Air Resources Laboratory (ARL) for the provision of the HYSPLIT transport and dispersion model
303 and/or READY website (<https://www.ready.noaa.gov>) used in this publication.

304 **Author Contribution**

305 Conceptualization of the study by AA. Design and execution of field campaigns by LK, AA, SG and MJG.
306 Management of Mt. Kenya GAW station and instrument calibration by DN, JK, CZ, CF & MS. Isotope analysis
307 by MEP. 1996/97 sampling campaign and sample analysis by TR. Data analysis by LK with support from AA,
308 ÖG, SLH and SG; Manuscript writing by LK with support from co-authors.

309 **Competing interests**

310 The authors declare no competing interests.

311 **Additional information**

312 Supplementary Information (SI) contain the flask-based CO measurement data for the 1996/97 and 2021 sampling
313 campaigns and the respective stable isotopes of CO (Table S1- S3).

314 Data from this study will be available in the Bolin Centre Database (bolin.su.se/data/).

315

316 **References**

317 Andersson, A.: Mechanisms for log normal concentration distributions in the environment, *Sci. Rep.*, 11(1), 1–7,

318 doi:10.1038/s41598-021-96010-6, 2021.

319 Andersson, A., Kirillova, E. N., Decesari, S., Dewitt, L., Gasore, J., Potter, K. E., Prinn, R. G., Rupakheti, M.,
320 De Dieu Ndikubwimana, J., Nkusi, J. and Safari, B.: Seasonal source variability of carbonaceous aerosols at the
321 Rwanda Climate Observatory, *Atmos. Chem. Phys.*, 20(8), 4561–4573, doi:10.5194/acp-20-4561-2020, 2020.

322 Brenninkmeijer, C. A. M.: Measurement of the abundance of ^{14}CO in the atmosphere and the $^{13}\text{C}/^{12}\text{C}$ and
323 $^{18}\text{O}/^{16}\text{O}$ ratio of atmospheric CO with applications in New Zealand and Antarctica, *J. Geophys. Res.*, 98(D6),
324 doi:10.1029/93jd00587, 1993.

325 Brenninkmeijer, C. A. M. and Röckmann, T.: Principal factors determining the $^{18}\text{O}/^{16}\text{O}$ ratio of atmospheric
326 CO as derived from observations in the southern hemispheric troposphere and lowermost stratosphere, *J.*
327 *Geophys. Res. Atmos.*, 102(21), 25477–25485, doi:10.1029/97jd02291, 1997.

328 Brenninkmeijer, C. A. M., Röckmann, T., Bräunlich, M., Jöckei, P. and Bergamaschi, P.: Review of progress in
329 isotope studies of atmospheric carbon monoxide, *Chemosph. - Glob. Chang. Sci.*, 1(1–3), 33–52,
330 doi:10.1016/S1465-9972(99)00018-5, 1999.

331 Buchholz, R. R., Worden, H. M., Park, M., Francis, G., Deeter, M. N., Edwards, D. P., Emmons, L. K., Gaubert,
332 B., Gille, J., Martínez-Alonso, S., Tang, W., Kumar, R., Drummond, J. R., Clerbaux, C., George, M., Coheur, P.
333 F., Hurtmans, D., Bowman, K. W., Luo, M., Payne, V. H., Worden, J. R., Chin, M., Levy, R. C., Warner, J.,
334 Wei, Z. and Kulawik, S. S.: Air pollution trends measured from Terra: CO and AOD over industrial, fire-prone,
335 and background regions, *Remote Sens. Environ.*, 256, 112275, doi:10.1016/j.rse.2020.112275, 2021.

336 Chen, K., Breitner, S., Wolf, K., Stafoggia, M., Sera, F., Vicedo-Cabrera, A. M., Guo, Y., Tong, S., Lavigne, E.,
337 Matus, P., Valdés, N., Kan, H., Jaakkola, J. J. K., Rytty, N. R. I., Huber, V., Scortichini, M., Hashizume, M.,
338 Honda, Y., Nunes, B., Madureira, J., Holobâcă, I. H., Fratanni, S., Kim, H., Lee, W., Tobias, A., Íñiguez, C.,
339 Forsberg, B., Åström, C., Ragettli, M. S., Guo, Y. L. L., Chen, B. Y., Li, S., Milojevic, A., Zanobetti, A.,
340 Schwartz, J., Bell, M. L., Gasparrini, A. and Schneider, A.: Ambient carbon monoxide and daily mortality: a
341 global time-series study in 337 cities, *Lancet Planet. Heal.*, 5(4), e191–e199, doi:10.1016/S2542-5196(21)00026-
342 7, 2021.

343 Crippa, M., Guizzardi, D., Muntean, M., Schaaf, E., Dentener, F., Van Aardenne, J. A., Monni, S., Doering, U.,
344 Olivier, J. G. J., Pagliari, V. and Janssens-Maenhout, G.: Gridded emissions of air pollutants for the period 1970-
345 2012 within EDGAR v4.3.2, *Earth Syst. Sci. Data*, 10(4), 1987–2013, doi:10.5194/essd-10-1987-2018, 2018.

346 Dasari, S., Andersson, A., Popa, M. E., Röckmann, T., Holmstrand, H., Budhavant, K. and Gustafsson, Ö.:
347 Observational Evidence of Large Contribution from Primary Sources for Carbon Monoxide in the South Asian
348 Outflow, *Environ. Sci. Technol.*, 56(1), 165–174, doi:10.1021/acs.est.1c05486, 2021.

349 DeWitt, H. L., Gasore, J., Rupakheti, M., Potter, K. E., Prinn, R. G., De Dieu Ndikubwimana, J., Nkusi, J. and
350 Safari, B.: Seasonal and diurnal variability in O₃, black carbon, and CO measured at the Rwanda Climate
351 Observatory, *Atmos. Chem. Phys.*, 19(3), 2063–2078, doi:10.5194/acp-19-2063-2019, 2019.

352 Duncan, B. N., Logan, J. A., Bey, I., Megretskaia, I. A., Yantosca, R. M., Novelli, P. C., Jones, N. B. and
353 Rinsland, C. P.: Global budget of CO, 1988 - 1997: Source estimates and validation with a global model, *J.*
354 *Geophys. Res. Atmos.*, 112(22), 1988–1997, doi:10.1029/2007JD008459, 2007.

355 Hedelius, J. K., Toon, G. C., Buchholz, R. R., Iraci, L. T., Podolske, J. R., Roehl, C. M., Wennberg, P. O.,
356 Worden, H. M. and Wunch, D.: Regional and Urban Column CO Trends and Anomalies as Observed by
357 MOPITT Over 16 Years, *J. Geophys. Res. Atmos.*, 126(5), 1–18, doi:10.1029/2020JD033967, 2021.

358 Henne, S., Junkermann, W., Kariuki, J. M., Aseyo, J. and Klausen, J.: Mount Kenya global atmosphere watch
359 station (MKN): Installation and meteorological characterization, *J. Appl. Meteorol. Climatol.*, 47(11), 2946–
360 2962, doi:10.1175/2008JAMC1834.1, 2008a.

361 Henne, S., Klausen, J., Junkermann, W., Kariuki, J. M., Aseyo, J. O. and Buchmann, B.: Representativeness and
362 climatology of carbon monoxide and ozone at the global GAW station Mt. Kenya in equatorial Africa, *Atmos.*
363 *Chem. Phys.*, 8(12), 3119–3139, doi:10.5194/acp-8-3119-2008, 2008b.

364 Keeling, C. D.: The concentration and isotopic abundances of atmospheric carbon dioxide in rural areas,
365 *Geochim. Cosmochim. Acta*, 13(4), 322–334, doi:10.1016/0016-7037(58)90033-4, 1958.

366 Kirago, L., Gustafsson, Ö., Gaita, S. M., Haslett, S. L., deWitt, H. L., Gasore, J., Potter, K. E., Prinn, R. G.,
367 Rupakheti, M., Ndikubwimana, J. de D., Safari, B. and Andersson, A.: Atmospheric Black Carbon Loadings and
368 Sources over Eastern Sub-Saharan Africa Are Governed by the Regional Savanna Fires, *Environ. Sci. Technol.*,
369 doi:10.1021/acs.est.2c05837, 2022a.

370 Kirago, L., Gatari, M. J., Gustafsson, Ö. and Andersson, A.: Black carbon emissions from traffic contribute
371 substantially to air pollution in Nairobi, Kenya, *Commun. Earth Environ.*, 3(1), 1–8, doi:10.1038/s43247-022-
372 00400-1, 2022b.

373 Kirago, L., Gatari, M. J., Gustafsson, Ö. and Andersson, A.: Large Contribution of Fossil Black Carbon to Air
374 Pollution in Nairobi , Kenya, *Commun. Earth Environ.*, 2022c.

375 Kulmala, M.: Build a global Earth observatory, *Nature*, 553(7686), 21–23, doi:10.1038/d41586-017-08967-y,
376 2018.

377 Lelieveld, J., Gromov, S., Pozzer, A. and Taraborrelli, D.: Global tropospheric hydroxyl distribution, budget and
378 reactivity, *Atmos. Chem. Phys.*, 16(19), 12477–12493, doi:10.5194/acp-16-12477-2016, 2016.

379 Mak, J. E. and Brenninkmeijer, C. A. M.: Compressed air sample technology for isotopic analysis of
380 atmospheric carbon monoxide, *J. Atmos. Ocean. Technol.*, 11(2), 425–431, doi:https://doi.org/10.1175/1520-
381 0426(1994)011%3C0425:CASTFI%3E2.0.CO;2, 1994.

382 Pathirana, S. L., Van Der Veen, C., Popa, M. E. and Röckmann, T.: An analytical system for stable isotope
383 analysis on carbon monoxide using continuous-flow isotope-ratio mass spectrometry, *Atmos. Meas. Tech.*,
384 8(12), 5315–5324, doi:10.5194/amt-8-5315-2015, 2015.

385 Petron, G.: Atmospheric CO at Mt. Kenya by Global Monitoring Laboratory, NOAA , dataset published as
386 CO_MKN_surface-flask_NOAA_ccgg at WDCGG ver. 2023-08-29-1326, ,
387 doi:<https://gaw.kishou.go.jp/search/file/0002-1005-3001-01-02-3001>, 2023.

388 Popa, M. E., Vollmer, M. K., Jordan, A., Brand, W. A., Pathirana, S. L., Rothe, M. and Röckmann, T.: Vehicle
389 emissions of greenhouse gases and related tracers from a tunnel study: CO : CO₂, N₂O : CH₄ : O₂ : Atios, and
390 the stable isotopes ¹³C and ¹⁸O in CO₂ and CO, *Atmos. Chem. Phys.*, 14(4), 2105–2123, doi:10.5194/acp-14-
391 2105-2014, 2014.

392 Röckmann, T., Brenninkmeijer, C. A. M., Saueressig, G., Bergamaschi, P., Crowley, J. N., Fischer, H. and
393 Crutzen, P. J.: Mass-independent oxygen isotope fractionation in atmospheric CO as a result of the reaction CO
394 + OH, *Science* (80-.), 281(5376), 544–546, doi:10.1126/science.281.5376.544, 1998.

395 Röckmann, T., Jöckel, P., Gros, V., Bräunlich, M., Possnert, G. and Brenninkmeijer, C. A. M.: Using ¹⁴C, ¹³C,
396 ¹⁸O and ¹⁷O isotopic variations to provide insights into the high northern latitude surface CO inventory, *Atmos.*
397 *Chem. Phys.*, 2, 147–159 [online] Available from: www.atmos-chem-phys.org/acp/2/147/, 2002.

398 Stein, A. F., Draxler, R. R., Rolph, G. D., Stunder, B. J. B., Cohen, M. D. and Ngan, F.: Noaa’s hysplit
399 atmospheric transport and dispersion modeling system, *Bull. Am. Meteorol. Soc.*, 96(12), 2059–2077,
400 doi:10.1175/BAMS-D-14-00110.1, 2015.

401 Szopa, S., Naik, V., Adhikary, B., Artaxo, P., Berntsen, T., Collins, W. D., Fuzzi, S., Gallardo, L., Kiendler, A.,
402 Scharr, Z., Klimont, Liao, H., Unger, N. and Zanis, P.: Short-Lived Climate Forcers. In *Climate Change 2021:*
403 *The Physical Science Basis. Contribution of Working Group I to the Sixth Assessment Report of the*
404 *Intergovernmental Panel on Climate Change.* [online] Available from: <https://www.ipcc.ch/>, 2021.

405 WHO: WHO Expert Consultation: Available evidence for the future update of the WHO Global Air Quality
406 Guidelines, Copenhagen, Denmark. [online] Available from: <http://www.euro.who.int/pubrequest>, 2016.

407 Worden, H. M., Anthony Bloom, A., Worden, J. R., Jiang, Z., Marais, E. A., Stavrou, T., Gaubert, B. and
408 Lacey, F.: New constraints on biogenic emissions using satellite-based estimates of carbon monoxide fluxes,
409 *Atmos. Chem. Phys.*, 19(21), 13569–13579, doi:10.5194/acp-19-13569-2019, 2019.

410 World Bank: Wood-Based Biomass Energy Development for Sub-Saharan Africa, Washington, D.C., 2011.

411 Zellweger, C., Hüglin, C., Klausen, J., Steinbacher, M., Vollmer, M. and Buchmann, B.: Inter-comparison of
412 four different carbon monoxide measurement techniques and evaluation of the long-term carbon monoxide time
413 series of Jungfraujoch, *Atmos. Chem. Phys.*, 9(11), 3491–3503, doi:10.5194/acp-9-3491-2009, 2009.

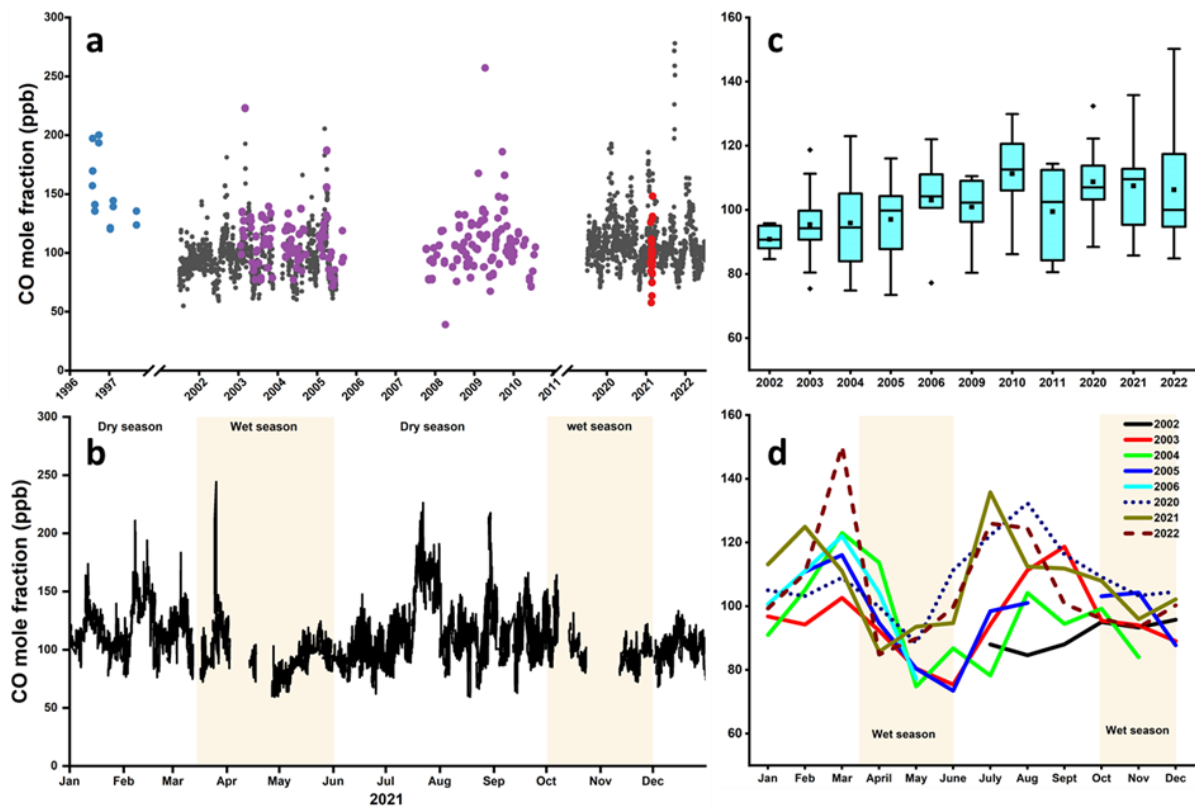
414 Zellweger, C., Steinbacher, M. and Buchmann, B.: GAW Report No. 256 / WCC-Empa Report No. 19/4. System
415 and Performance Audit of Surface Ozone, Carbon Monoxide, Methane, and Carbon Dioxide at the Global GAW
416 Station Mt. Kenya, Kenya, Geneva. [online] Available from:
417 https://library.wmo.int/index.php?lvl=notice_display&id=21780, 2020.

418 Zhang, J. J., Wei, Y. and Fang, Z.: Ozone pollution: A major health hazard worldwide, *Front. Immunol.*,
419 10(OCT), 1–10, doi:10.3389/fimmu.2019.02518, 2019.

420 Zheng, B., Chevallier, F., Ciais, P., Yin, Y. and Wang, Y.: On the Role of the Flaming to Smoldering Transition
421 in the Seasonal Cycle of African Fire Emissions, *Geophys. Res. Lett.*, 45(21), 11,998-12,007,
422 doi:10.1029/2018GL079092, 2018.

423 Zheng, B., Chevallier, F., Yin, Y., Ciais, P., Fortems-Cheiney, A., Deeter, M. N., Parker, R. J., Wang, Y.,
424 Worden, H. M. and Zhao, Y.: Global atmospheric carbon monoxide budget 2000-2017 inferred from multi-
425 species atmospheric inversions, *Earth Syst. Sci. Data*, 11(3), 1411–1436, doi:10.5194/essd-11-1411-2019, 2019.

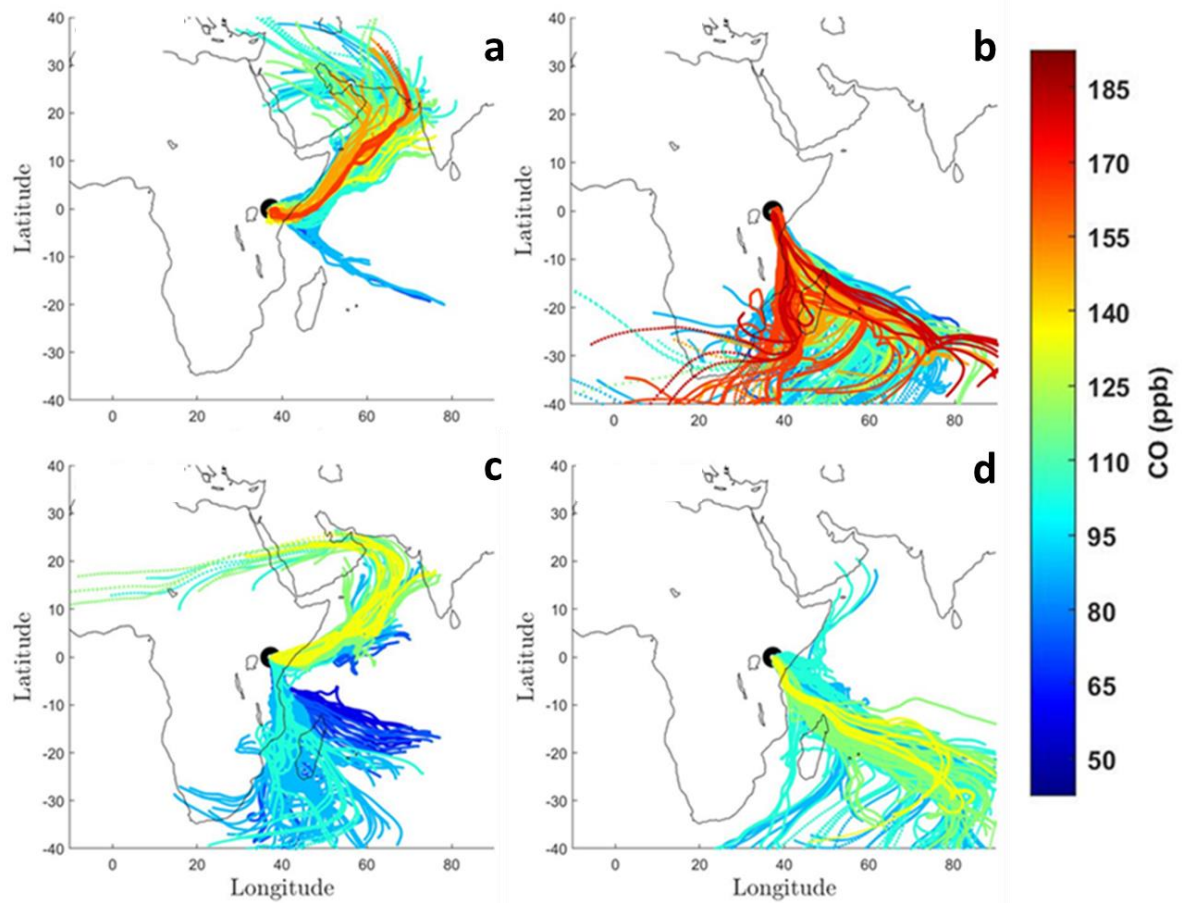
426



427

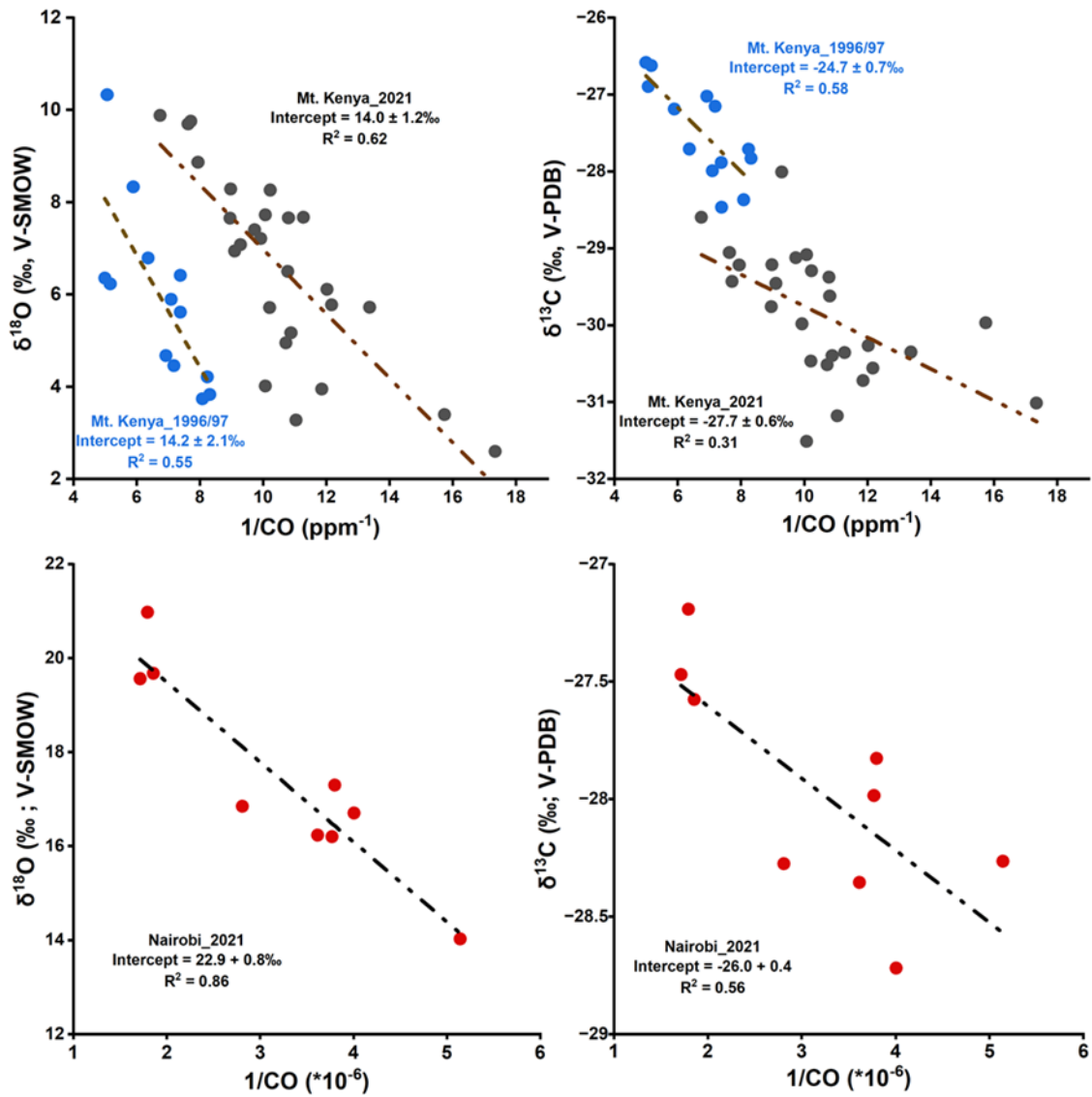
428 **Figure 1:** Time series of CO mole fractions at Mt. Kenya GAW station. a) Daily-resolution continuously measured CO
 429 mole fraction (Picarro) at Mt. Kenya GAW is represented by black dots. The CO data was retrieved from the WMO's-
 430 WDCGG database covering 2002- 2021. Different instrumentations were used over time, but similar instrumental
 431 calibration, quality control, and assurance protocols were applied. Flask-based measurements by NOAA at the station
 432 are presented in purple symbols, while flask samples during 1996/97 campaigns are shown as blue dots and flask
 433 samples from the 2021 campaign are shown in red symbols, in good agreement with the online measurements, as shown
 434 in SI Figure S4. b) Variations of CO mole fractions for the year 2021. The prevailing typical weather conditions are
 435 indicated. c) Annual averaged CO mixing ratios. The boxes represent the 25th and 75th quantiles, and the black line
 436 represents the median value. The bottom/top whiskers are the minimum and maximum values, respectively, while
 437 diamonds represent the outliers. d) Inter-annual cycles of monthly averaged CO mole fractions (coloured lines represent
 438 individual years).

439



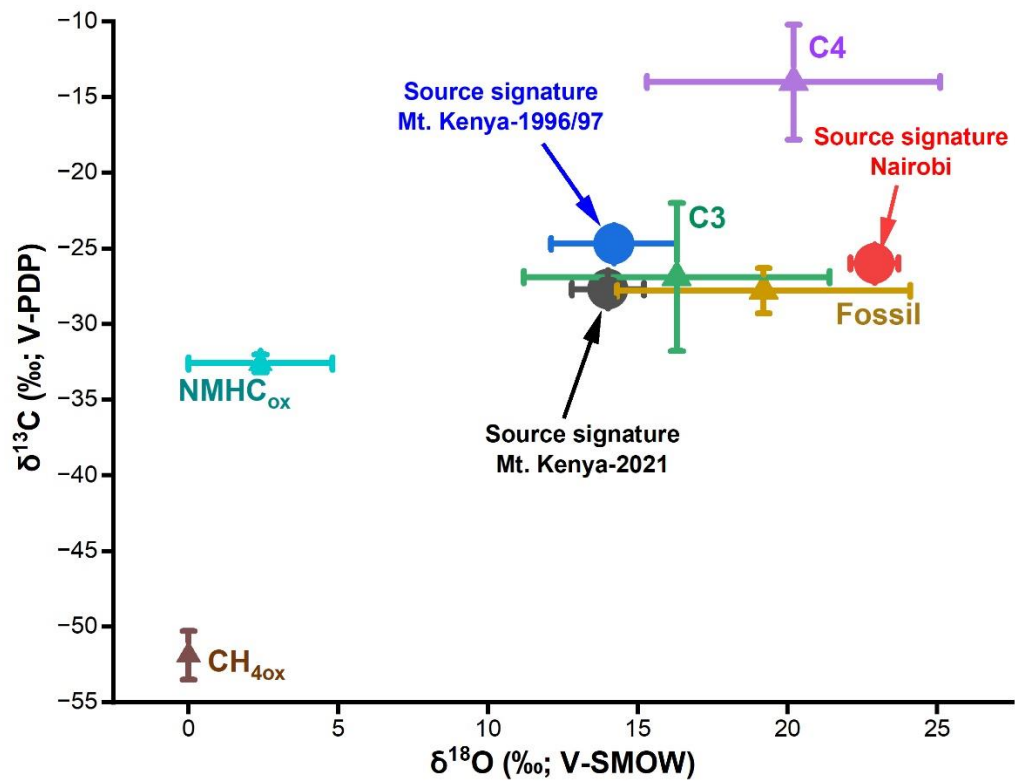
440

441 **Figure 2: Seasonal changes in CO concentration-coded back trajectories intercepted at Mt. Kenya; (a) December –**
 442 **February 2021, (b) June – August 2021, (c) March – May 2021, and (d) September – November 2021. (a) December –**
 443 **February, (b) June – August, (c) March – May, and (d) September – November. Ten days air masses back trajectories**
 444 **are calculated at an arrival height of 100 m above ground level.**



445

446 **Figure 3: The Keeling relation plots (i.e., signatures of the two isotopic systems vs the inverse of the measured CO mole**
 447 **fraction) for Mt. Kenya (top panel) and Nairobi (bottom panel). The y-intercept in the Keeling relationship represents**
 448 **the source signature.**



449

450 **Figure 4:** Stable isotope ($\delta^{13}\text{C}$ and $\delta^{18}\text{O}$) source signatures of CO for Nairobi and Mt. Kenya (2021 and 1996/97), and
 451 the source end members. The source end members are adopted from Brenninkmeijer et al. (1999).